nature physics

ARTICLES

https://doi.org/10.1038/s41567-018-0097-9

# Charge quantum interference device

S. E. de Graaf[1*], S. T. Skacel[2], T. Hönigl-Decrinis[1,3], R. Shaikhaidarov[3,4], H. Rotzinger[2], S. Linzen[5], M. Ziegler[5], U. Hübner[5], H.-G. Meyer[5], V. Antonov[3,6], E. Il'ichev[5,7], A. V. Ustinov[2,7], A. Ya. Tzalenchuk[1,3] and O. V. Astafiev[1,3,4,7]

**The demonstration of coherent quantum phase slips (CQPS) in disordered superconductors has opened up a new route towards exploring the fundamental charge–phase duality in superconductors, with the promise of devices with new functionalities and a robust quantum current standard based on CQPS. Here we demonstrate a device that integrates several CQPS junctions: the charge quantum interference device. The charge quantum interference device becomes the dual of the well-known superconducting quantum interference device, and is a manifestation of the Aharonov–Casher effect in a continuous superconducting system devoid of dielectric barriers.**

Superconductivity in metallic nanowires is strongly influenced by fluctuations of the superconducting order parameter[1]. Thermally activated phase slips (TAPS) are dominant[2] near the superconducting transition temperature, $T_c$. Well below $T_c$ the phase of a homogeneous superconducting wire can slip by $2\pi$ due to quantum tunnelling, a process analogous to Cooper-pair tunnelling in Josephson junctions[3]. The notion of coherent phase slips in nanowires proposed by Mooij and Nazarov[4] was supported by experiments by Astafiev et al.[5] with wires made of nominally homogeneous superconducting material. Such CQPS, carried by tunnelling of magnetic fluxons across a superconducting wire, enable devices based on quantum interference effects, opening a route towards a wide range of quantum devices dual to those that can be implemented with Josephson junctions[4,6,7].

Quantum interference of Cooper pairs in flux-based superconducting quantum interference devices (SQUIDs) was demonstrated soon after the discovery of the Josephson effect[8] and has since become a cornerstone of superconducting electronics. Another cornerstone is the locking of the phase across the Josephson junction to an external microwave field, resulting in Shapiro steps at quantized voltages[9]. This effect is used in high-frequency amplifiers and detectors, and as the basis for the quantum voltage standard, which today underpins the electronics industry[10]. The main motivation for studying CQPS and dual superconducting devices has so far been the promise of a robust quantum current standard based on so-called dual Shapiro steps[4,11–13], complementary to the Josephson voltage standard. Although this particular goal has not yet been achieved, the experimental observation of CQPS in superconducting nanowires[5] has advanced the understanding of one-dimensional superconductivity and coherence in disordered superconductors[14,15] to the level where dual superconducting electronics has now become a possibility.

Conventional d.c. SQUIDs can be viewed as a specific implementation of the Aharonov–Bohm (AB) effect[16], where interference of the wavefunction of a moving charged particle occurs when it encircles a flux (Fig. 1a). In contrast, the Aharonov–Casher (AC) effect, where the interference of fluxon trajectories occurs around a static charge[17], is dual to the AB effect. The AC effect has previously been observed in a variety of particle and solid-state systems[18–21] and in Josephson junction arrays[22–26]. Here we demonstrate the AC effect in a nominally continuous superconductor. Our device comprises two series CQPS junctions in which we achieve charge-controlled interference of fluxon tunnelling in a device exactly dual to the SQUID. We call this device the charge quantum interference device (CQUID). This coherent charge-sensitive interferometer demonstrates the potential of CQPS devices previously explored only through the approximate[4] self-duality of Josephson junction circuits[12,22,27–31]. Such arrays of Josephson junctions have been shown to be a challenging complementary route towards a quantum current standard based on quantum phase slips[32].

In the CQUID, schematically shown in Fig. 1b, flux coherently tunnels across two narrow constrictions in a superconducting wire that we conclude is continuous in the superconducting order parameter (see evidence in Supplementary Information). The two constrictions, of size ~30nm × 50 nm, are connected in series and made out of a continuous ~3.3-nm-thick NbN film. These constrictions provide well-defined points with an increased phase slip amplitude[15]. The wider, ~100 nm, region ('island') between the constrictions is coupled through the capacitance $C_g$ to a gate electrode. The island is made large enough to prohibit phase slips, but small enough to minimize its self-capacitance shunting the CQUID. Such a shunt capacitance would reduce the impedance and renormalize the phase-slip amplitude of the device.

The charge induced by the gate potential $V_g$ controls the interference of the phase-slip amplitudes, with a period of $2e$, in much the same way as the effective Josephson energy in the SQUID is tuned by an external magnetic flux, with a period of $\Phi_0$, the flux quantum. Each interferometer becomes indistinguishable from its dual counterpart by the dual single-particle exchange (Cooper pair or fluxon) with the following additional substitutions: current (Cooper-pair flow) ↔ voltage (flux flow), charge ↔ magnetic flux, Josephson energy ↔ phase-slip energy and insulator ↔ superconductor[4]. This also implies that the lack of flux quantization in the SQUID translates to the absence of charge quantization in the dual device, and the induced charge on the island (normalized to $2e$) precisely follows $q = C_g V_g / 2e$.

[1]National Physical Laboratory, Teddington, UK. [2]Physikalisches Institut, Karlsruhe Institute of Technology, Karlsruhe, Germany. [3]Department of Physics, Royal Holloway University of London, Egham, UK. [4]Moscow Institute of Physics and Technology, Dolgoprudny, Russia. [5]Leibniz Institute of Photonic Technology, Jena, Germany. [6]Skolkovo Institute of Science and Technology, Moscow, Russia. [7]Russian Quantum Center, National University of Science and Technology MISIS, Moscow, Russia. *e-mail: sdg@npl.co.uk

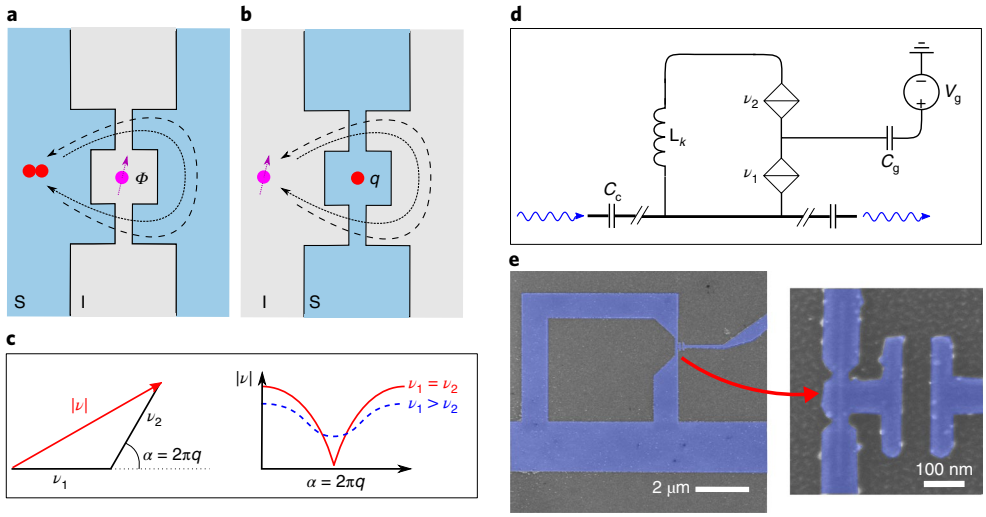


**Fig. 1 | Duality and sample design. a**, Interference effect in a SQUID. The flow of Cooper pairs around a flux results in critical current fluctuations. Solid and dashed black arrows indicate the two different particle trajectories in the device, and I and S denote insulator and superconductor, respectively. **b**, Schematic representation of the dual CQUID. The phase interference results from flow of flux around a charge. **c**, Phase-slip amplitude interference represented as two complex phasors. Equal phase-slip amplitudes of the two junctions result in a $|\cos 2\pi q|$ dependence of the total measured phase-slip rate (solid line), while dissimilar amplitudes will yield a weaker dependence (dashed line) tending towards a sinusoidal dependence. **d**, Circuit representation of our device. **e**, False-colour electron micrograph of the device and a close-up on the CQPS junctions and the gated island. Blue indicates the NbN film.

In much the same way as the insulator in a superconductor–insulator–superconductor (SIS) junction provides a tunnel barrier for Cooper pairs (but not to fluxons), a continuous superconductor provides a tunnel barrier for fluxons (but not for Cooper pairs). Observation of CQPS requires a low barrier for flux tunnelling across the superconductor, realized by a high kinetic inductance. This is achieved in highly disordered superconducting films close to the superconductor–insulator transition (SIT)[14,15]. The same magnitude of the phase-slip amplitude can be realized in a wider constriction for superconductors close to the SIT, easing fabrication requirements and increasing reproducibility due to the exponential dependence of phase-slip amplitude on constriction width[14]. By using atomic layer deposition (ALD)-grown NbN films[33–35], we can now controllably make high-quality films that are very close to the SIT, enabling fabrication of multiple very similar CQPS constrictions in the same device using conventional nanofabrication techniques. We have verified the continuity of the superconducting order parameter in our films in independent measurements on microbridges. For the CQUID devices presented here we also confirmed that the phase-slip energy in the CQUID persists up to magnetic fields much larger than would be possible for a small-area Josephson junction, confirming that our CQPS junctions are indeed constrictions in a continuous film. We refer the reader to the Supplementary Information for further details.

Direct current (d.c.) transport measurements are essential for the realization of a current standard based on CQPS[4,13,31,36–38]; however, these are often complicated by incoherent effects such as Coulomb blockade and dissipation. To demonstrate CQPS interference in the CQUID we instead follow the methodology of previous studies[5,14,15] and use microwave spectroscopy, which provides a tool for measuring the tunnelling energy in quantum systems. In particular, the Cooper pair box connected to a reservoir via a SQUID allows one to control and measure the Cooper-pair tunnelling energy (Josephson energy) of the SQUID[39]. We develop an exact dual measurement circuit: the CQUID is implemented in a loop with a high but finite inductance. The resulting flux states provides a degree of freedom orthogonal to the energy spectrum of the CQUID and the fluxon flow due to CQPS. The circuit allows us to directly measure the tunnelling energy of the CQUID (tunnelling energy of fluxons); see Supplementary Information for details. In addition, a high-impedance environment for flux tunnelling is achieved by embedding the loop in a $\lambda/2$ superconducting resonator, made from the same NbN film. The resonator allows for direct readout of the energy spectrum of the device by dispersive microwave spectroscopy[5,14,15].

The reduced Hamiltonian describing our device in the flux basis is $H=-E_L\sigma_z/2-E_s\sigma_x/2$ (refs [6,40]), where $\sigma_i$ are the Pauli matrices, $E_s=h\,|\nu_{tot}|$ is the coupling energy due to the phase-slip amplitude $\nu_{tot}$ and $E_L=2I_p\delta\Phi$ is the inductive energy due to the persistent current $I_p=\Phi_0/2L_k$ in the loop with kinetic inductance $L_k$ and $\delta\Phi=\Phi_{ext}-(N+1/2)\Phi_0$. $N$ is the number of magnetic flux quanta $\Phi_0$ in the loop subjected to a magnetic flux $\Phi_{ext}$ tuned by an external solenoid. The energy difference between the ground and the first excited state of the diagonalized Hamiltonian is $\Delta E=((2I_p\delta\Phi)^2+E_s^2)^{1/2}$. When introducing two discrete arbitrary phase-slip junctions in series separated by an island, the lowest energy level transition in the ring becomes

$$\Delta E=\sqrt{(2I_p\delta\Phi)^2+h^2\,|\nu_1+\nu_2e^{i2\pi q}|^2} \qquad (1)$$

where we use $\nu_{tot}=\nu_1+\nu_2e^{i2\pi q}$ (refs [22,30,41]). $\nu_1$ and $\nu_2$ are the bare phase-slip amplitudes for the two junctions, respectively. Importantly, the phase-slip rate depends only on the gate-induced charge. This is a direct result of the non-quantized charge, and Cooper pairs are not localized on the island. The expected $2e$-periodic oscillations due to the induced charge on the island are a result of the phase-slip amplitude interference across the two junctions. We note that equation (1) applies to both CQPS and Josephson junction chains, and a distinction of the underlying physics could not be based solely on equation (1). We refer the reader to our Supplementary Information for a thorough discussion on the nature and homogeneity of our CQPS junctions.

The case of symmetric phase slip amplitudes ($\nu_1=\nu_2$) reduces for $\delta\Phi=0$ to $\Delta E\propto|\cos\pi q|$, in exact duality to the flux-modulated critical current of a magnetic SQUID with two identical Josephson junctions. For certain values of $q$ we would thus expect the transition

energy to be suppressed to zero. For largely dissimilar phase-slip amplitudes ($\nu_1 \gg \nu_2$), or in the presence of non-trivial flux bias $\delta\Phi \neq n\Phi_0$ (where $n$ is an integer number), the variation in $\Delta E$ due to the induced charge instead resembles a sinusoidal dependence, as sketched in Fig. 1c. We now proceed to the measurements of our device, which are in very good agreement with these expectations.

Figure 2a,b shows the measured energy level spectroscopy data as a function of magnetic flux for two different applied gate voltages. From the asymptotically linear dependence of the energy level transitions on magnetic flux, we extract $I_p = 30$ nA and $L_k = 33$ nH, corresponding to the inductance per square of the NbN film $L_\square = 1.35$ nH. Bardeen–Cooper–Schrieffer (BCS) theory underestimates $L_k$ near the SIT[42]. From the normal state per square resistance $R_\square = 2.3\,\mathrm{k\Omega}$ measured above $T_c$, we get $L_\square = \hbar R_\square/(\pi\Delta_{bcs}) = 0.67$ nH for $T_c = 4.7$ K, different by a factor of two. Figure 2c shows the full response of the energy levels due to the induced charge on the island at $\delta\Phi = 0$. Notably, for each gate voltage we find two spectroscopic lines that deviate in phase from each other in gate voltage. These lines are shifted in charge by exactly half-a-period, which is explained by charge interference (AC effect) and the presence of non-equilibrium quasiparticles. A change in the number of non-equilibrium quasiparticles ($N_{qp}$) present on the island will chan ge the overall island charge by $1e$ and the AC phase by $\pi$. Depending on the charge number parity of the island[43,44], we observe two different parity bands according to $\nu_{tot} = \nu_1 + (-1)^{N_{qp}}\nu_2 e^{i2\pi q}$. This is similar to what has been observed in charge qubits[45]. In the complex-amplitude representation of the phase-slip amplitude of equation (1) shown in Fig. 2e, such parity shifts result in two phase-slip amplitudes rotated by exactly $\pi$. The two bands are maximally separated at an induced island charge of precisely $q = ne$, where $n$ is an integer.

The oscillations provide compelling evidence for flux interference, the fundamental mechanism on which the CQUID is based, and are a demonstration of the AC effect in a solid-state system without insulating tunnelling barriers[18,22]. This is further shown by Fig. 2d, showing the fit of the data in Fig. 2c to equation (1). We extract the two phase-slip amplitudes $\nu_1 = 9.2$ GHz and $\nu_2 = 3.3$ GHz. This strong similarity in phase-slip amplitudes allows us to accurately compare the CQUID operation with theoretical predictions.

We may express the phase-slip energy of a single constriction in terms of the dimensionless conductance $g_\xi = R_q/R_\xi$ of a wire segment of length $\xi$, where $R_q = h/4e^2$ is the superconducting resistance quantum[1]: $E_s = (\Delta g_\xi)\exp(-a g_\xi)$. Here the dimensionless parameter[6,46] $a \approx 0.3$ is only weakly dependent on the environment of the phase-slip junction. For the measured phase-slip amplitudes of 3.3 GHz and 9.2 GHz and for junction dimensions of 46 nm × 30 nm and 39 nm × 30 nm, respectively, we obtain $a \approx 0.29$, in excellent agreement with the observed dimensions and the expected value for $a$.

As we move the flux bias away from the degeneracy point we expect that the variation in transition energy with induced charge on the island is suppressed. In Fig. 3a we show the difference in transition energy at the maximum and minimum of equation (1) with respect to the gate-induced charge $q$ as a function of flux detuning $\delta\Phi_0$, and in Fig. 3b we show the measured and expected deviation of equation (1) from a pure sinusoidal dependence of $\Delta E$ on $q$. Both data sets are in exceptionally good agreement with equation (1). The transition linewidth is $\delta E/h = 200$ MHz in the weak-drive limit for both the even and odd parity modes, and their occupation probabilities are the same (Fig. 3c). This linewidth is similar to that obtained in previous experiments where CQPS has been studied[5,14,15].

The origin of the parity fluctuations can be understood by considering the nature of the junctions in the device. We may introduce an arbitrary number of quasiparticles on the CQUID island without incurring any additional electrostatic energy. Instead, the normal-state resistance determines the time that a non-equilibrium quasiparticle spends on the island (in the absence of recombination, which is parity-conserving). We may estimate the shortest

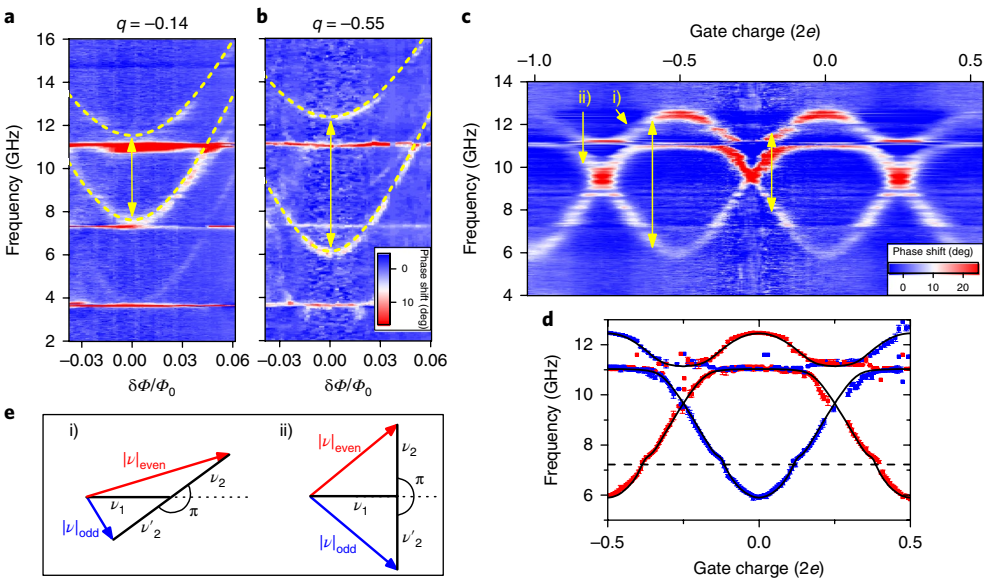


**Fig. 2 | Energy level spectroscopy of the CQUID. a**,**b**, Spectroscopy data of the same device for two different applied gate voltages (different island charge $q$). Readout is performed by two-tone microwave spectroscopy with a weak probe tone at the fundamental resonance frequency of 3.7 GHz. The resonator had a quality factor of 600. Dashed lines are fits to equation (1); the only difference between the four dashed lines is the charge; all other fitting parameters are the same. Other parabolic spectroscopic lines visible are due to higher-order energy level transitions, and horizontal lines are resonator modes. **c**, Two-tone microwave spectroscopy phase variation data taken at $\delta\Phi = 0$ as a function of induced charge on the island. Double-sided arrows indicate the identical working points in **a** and **b**. **d**, Extracted transition frequencies for the even (red) and odd (blue) parity states. Solid lines are fits to equation (1) where we have also included hybridization with the third resonance mode at 11 GHz (coupling strength $g = 225$ MHz) and weak coupling to the second resonance mode (dashed line at 7.3 GHz, $g \approx 70$ MHz). Error bars indicate 95% confidence bounds to the fits of peak positions in **c**. **e**, Geometric construction of the two parity states even (red) and odd (blue) in the CQUID shifted by a phase $\pi$ in the complex plane; (i) and (ii) are for the two different gate charges indicated in **c**.

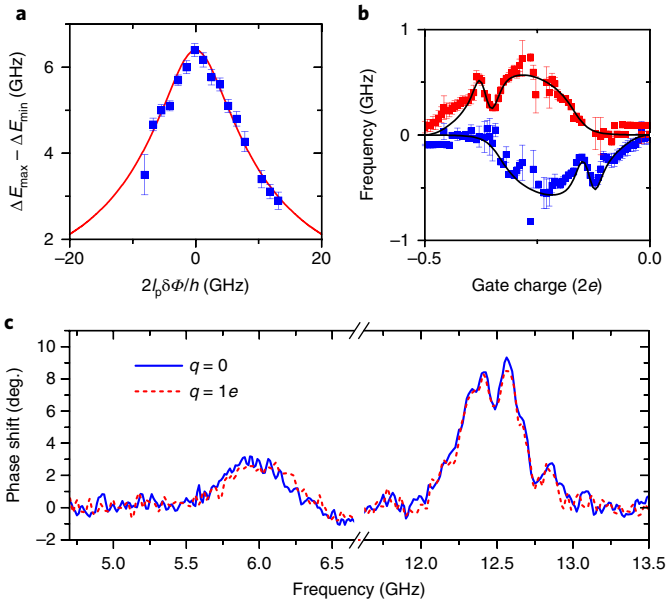


**Fig. 3 | Fit to theory and parity state population. a**, The measured maximum difference in transition frequency, obtained at induced gate charges of 0 and 1e, respectively, as a function of flux detuning from the degeneracy point $\delta\Phi = 0$. Error bars are observed transition linewidths. The red solid line is a fit to equation (1). **b**, The deviation of the two lower modes from a pure sinusoidal gate dependence of $E_s(q)$. The sharp kink is due to the coupling to the second resonance mode. Error bars indicate 95% confidence bounds to the fits of peak positions in Fig. 2c. **c**, Two-tone phase response for two induced gate charges showing equal populations of the two parity states. Differences in high- and low-frequency peak amplitudes are due to different coupling strengths to the resonator mode.

quasiparticle residence time on the island as $\tau_{qp} \approx e^2 R_\square V \rho \approx 2\,\mathrm{ns}$, where $\rho = 3.8 \times 10^{47}\,\mathrm{J^{-1}\,m^{-3}}$ (ref. [47]) is the density of states in NbN at the Fermi energy and $V \approx 10^{-22}\,\mathrm{m^3}$ is the volume of the island. Thus, in the presence of non-equilibrium quasiparticles in the leads, we expect to have a rapidly fluctuating number of quasiparticles $N_{qp}$ on the CQUID island, leading to the observed behaviour of equal probabilities for the two parities over the much longer measurement timescale.

The quasiparticle dwell time is comparable to the coherence time $\tau \simeq 5\,\mathrm{ns}$ we observe in our time-averaged measurements, extracted from the transition linewidth.

In addition to parity fluctuations, we observe large fractional charge jumps on a timescale of ~1 hour due to charge fluctuators in the surrounding dielectrics, a clear indication that offset charge fluctuations in long wires will affect the coherences and phase-slip amplitudes, analogous to what has been found for Josephson junction chains[32,48].

We have demonstrated control of the interference of coherent quantum phase-slip amplitudes in a charge quantum interference device comprised of two CQPS junctions. The excellent agreement with theory and large response due to the induced island charge is compelling evidence for the AC effect in a continuous highly disordered superconducting system. This demonstration of duality and the CQUID is an important step towards a future quantum current standard based on CQPS; however, the observed strong quasiparticle poisoning may provide an additional obstacle towards its realization. Quasiparticle poisoning may lead to a spurious quasiparticle current and perturbations to the phase locking of Bloch oscillations[48]. Quasiparticle poisoning is thus an engineering challenge that needs to be addressed using quasiparticle trapping and elimination techniques. By placing the coherent CQUID in a high-impedance environment for d.c. measurements it could be used as a route towards a CQPS-based current standard.

## Methods

Methods, including statements of data availability and any associated accession codes and references, are available at https://doi.org/10.1038/s41567-018-0097-9.

Received: 21 July 2017; Accepted: 2 March 2018;
Published online: 09 April 2018

## References

1. Arutyunov, K. Y., Golubev, D. S. & Zaikin, A. D. Superconductivity in one dimension. *Phys. Rep.* **464**, 1–70 (2008).
2. McCumber, D. E. & Halperin, B. I. Time scale of intrinsic resistive fluctuations in thin superconducting wires. *Phys. Rev. B* **1**, 1054–1070 (1970).
3. Martinis, J. M., Devoret, M. H. & Clarke, J. Experimental tests for the quantum behavior of a macroscopic degree of freedom: the phase difference across a Josephson junction. *Phys. Rev. B* **35**, 4682–4698 (1987).
4. Mooij, J. E. & Nazarov, Y. V. Superconducting nanowires as quantum phase-slip junctions. *Nat. Phys.* **2**, 169–172 (2006).
5. Astafiev, O. V. et al. Coherent quantum phase slip. *Nature* **484**, 355–358 (2012).
6. Mooij, J. E. & Harmans, C. J. P. M. Phase-slip flux qubits. *New. J. Phys.* **7**, 219 (2005).
7. Hriscu, A. M. & Nazarov, Y. V. Coulomb blockade due to quantum phase slips illustrated with devices. *Phys. Rev. B* **83**, 174511 (2011).
8. Jaklevic, R. C., Lambe, J., Silver, A. H. & Mercereau, J. E. Quantum interference effects in Josephson tunneling. *Phys. Rev. Lett.* **12**, 159–160 (1964).
9. Shapiro, S. Josephson currents in superconducting tunneling: The effect of microwaves and other observations. *Phys. Rev. Lett.* **11**, 80–82 (1963).
10. Kohlmann, J., Behr, R. & Funck, T. Josephson voltage standards. *Meas. Sci. Tech.* **14**, 1216–1228 (2003).
11. Gallop, J. C. *SQUIDs, the Josephson Effects and Superconducting Electronics* (IOP Publishing Ltd., Bristol, 1990).
12. Ergül, A. et al. Localising quantum phase slips in one-dimensional Josephson junction chains. *New. J. Phys.* **15**, 095014 (2013).
13. Webster, C. H. et al. NbSi nanowire quantum phase slip circuits: dc supercurrent blockade, microwave measurements, and thermal analysis. *Phys. Rev. B* **87**, 144510 (2013).
14. Peltonen, J. T. et al. Coherent flux tunneling through NbN nanowires. *Phys. Rev. B* **88**, 220506 (2013).
15. Peltonen, J. T. et al. Coherent dynamics and decoherence in a superconducting weak link. *Phys. Rev. B* **94**, 180508 (2016).
16. Aharonov, Y. & Bohm, D. Significance of electromagnetic potentials in the quantum theory. *Phys. Rev.* **115**, 485–491 (1959).
17. Aharonov, Y. & Casher, A. Topological quantum effects for neutral particles. *Phys. Rev. Lett.* **53**, 319–321 (1984).
18. Elion, W. J., Wachters, J. J., Sohn, L. L. & Mooij, J. E. Observation of the Aharonov–Casher effect in vortices in Josephson-junction arrays. *Phys. Rev. Lett.* **71**, 2311–2314 (1993).
19. Cimmino, A. et al. Observation of the topological Aharonov–Casher phase shift by neutron interferometry. *Phys. Rev. Lett.* **63**, 380–383 (1989).
20. Sangster, K., Hinds, E. A., Barnett, S. M. & Riis, E. Measurement of the Aharonov–Casher phase in an atomic system. *Phys. Rev. Lett.* **71**, 3641–3644 (1993).
21. König, M. et al. Direct observation of the Aharonov–Casher phase. *Phys. Rev. Lett.* **96**, 076804 (2006).
22. Pop, I. M. et al. Experimental demonstration of Aharanov–Casher interference in a Josephson junction circuit. *Phys. Rev. B* **85**, 094503 (2012).
23. Bell, M. T., Zhang, W., Ioffe, L. B. & Gershenson, M. E. Spectroscopic evidence of the Aharonov–Casher effect in a Cooper pair box. *Phys. Rev. Lett.* **116**, 107002 (2016).
24. Born, D. et al. Reading out the state inductively and microwave spectroscopy of an interferometer-type charge qubit. *Phys. Rev. B* **70**, 180501 (2004).
25. Manucharyan, V. E., Koch, J., Glazman, L. I. & Devoret, M. H. Fluxonium: Single Cooper-pair circuit free of charge offsets. *Science* **326**, 113–116 (2009).
26. Manucharyan, V. E. et al. Evidence for coherent quantum phase slips across a Josephson junction array. *Phys. Rev. B* **85**, 024521 (2012).
27. Masluk, N. A., Pop, I. M., Kamal, A., Minev, Z. K. & Devoret, M. H. Microwave characterisation of Josephson junction arrays: Implementing a low loss superinductance. *Phys. Rev. Lett.* **109**, 137002 (2012).
28. Kerman, A. J. Fluxcharge duality and topological quantum phase fluctuations in quasi-one-dimensional superconductors. *New. J. Phys.* **15**, 105017 (2013).

29. Guichard, W. & Hekking, F. W. J. Phase-charge duality in Josephson junction circuits: Role of inertia and effect of microwave irradiation. *Phys. Rev. B* **81**, 064508 (2010).
30. Friedman, J. R. & Averin, D. V. Aharonov–Casher-effect suppression of macroscopic tunneling of magnetic flux. *Phys. Rev. Lett.* **88**, 050403 (2002).
31. Weißl, T. et al. Bloch band dynamics of a Josephson junction in an inductive environment. *Phys. Rev. B* **91**, 014507 (2015).
32. Cedergren, K. et al. Insulating Josephson junction chains as pinned Luttinger liquids. *Phys. Rev. Lett.* **119**, 167701 (2017).
33. Linzen, S. et al. Structural and electrical properties of ultrathin niobium nitride films grown by atomic layer deposition. *Supercond. Sci. Technol.* **30**, 035010 (2017).
34. Ziegler, M. et al. Superconducting niobium nitride thin films deposited by metal organic plasma-enhanced atomic layer deposition. *Supercond. Sci. Technol.* **26**, 025008 (2013).
35. Ziegler, M. et al. Effects of plasma parameter on morphological and electrical properties of superconducting NbN fabricated by MO-PEALD. *IEEE Trans. Appl. Supercond.* **27**, 7501307 (2017).
36. Hongisto, T. T. & Zorin, A. B. Single-charge transistor based on the charge–phase duality of a superconducting nanowire. *Phys. Rev. Lett.* **108**, 097001 (2012).
37. Lehtinen, J. S., Zakharov, K. & Arutyunov, K. Y. Coulomb blockade and Bloch oscillations in superconducting Ti nanowires. *Phys. Rev. Lett.* **109**, 187001 (2012).
38. Kafanov, S. & Chtchelkatchev, N. M. Single flux transistor: The controllable interplay of coherent quantum phase slip and flux quantization. *J. Appl. Phys.* **114**, 073907 (2013).
39. Nakamura, Y., Pashkin, Y. A. & Tsai, J. S. Coherent control of macroscopic quantum states in a single-Cooper-pair box. *Nature* **398**, 786–788 (1999).
40. Hu, Z., Tie-Fu, L., Jian-She, L. & Wai, C. Charge-related SQUID and tunable phase-slip flux qubit. *Chinese Phys. Lett.* **31**, 030303 (2014).
41. Matveev, K. A., Larkin, A. I. & Glazman, L. I. Persistent current in superconducting nanorings. *Phys. Rev. Lett.* **89**, 096802 (2002).
42. Sacépé, B. et al. Localization of preformed Cooper pairs in disordered superconductors. *Nat. Phys.* **7**, 239–244 (2011).
43. Eiles, T. M., Martinis, J. M. & Devoret, M. H. Even–odd asymmetry of a superconductor revealed by the Coulomb blockade of Andreev reflection. *Phys. Rev. Lett.* **70**, 1862–1865 (1993).
44. Hekking, F. W. J., Glazman, L. I., Matveev, K. A. & Shekhter, R. I. Coulomb blockade of two-electron tunneling. *Phys. Rev. Lett.* **70**, 4138–4141 (1993).
45. Sun, L. et al. Measurements of quasiparticle tunneling dynamics in a band-gap-engineered transmon qubit. *Phys. Rev. Lett.* **108**, 230509 (2012).
46. Vanjevic, M. & Nazarov, Y. V. Quantum phase slips in superconducting wires with weak homogeneities. *Phys. Rev. Lett.* **108**, 187002 (2012).
47. Semenov, A. D., Goltsman, G. N. & Korneev, A. A. Quantum detection by current carrying superconducting film. *Phys. C* **351**, 349–356 (2001).
48. Vora, H., Kautz, R. L., Nam, S. W. & Aumentado, J. Modeling Bloch oscillations in nanoscale Josephson junctions. *Phys. Rev. B* **96**, 054505 (2017).


## Acknowledgements

This work was supported by the UK government's Department for Business, Energy and Industrial Strategy. We thank Y. Nazarov and A. Semenov for fruitful discussions. S.T.S. thanks S. Diewald and L. Radtke for their technical support during fabrication and acknowledges support from the Heinrich Böll Foundation and the KHYS. This work was partially supported by the Increase Competitiveness Program of the NUST MISiS (grants no. K2-2015-002 and 2-2016-051).

## Author contributions

O.V.A., S.E.d.G. and A.Y.T. conceived the experiment. S.E.d.G. designed the samples, performed the measurements with assistance from S.T.S., T.H.-D., R.S., V.A. and O.V.A., and analysed the data. S.L., M.Z., U.H., H.G.M. and E.I. developed the thin-film technology. S.T.S. fabricated the samples with assistance from H.R. and R.S. S.E.d.G. wrote the manuscript with input from O.V.A., S.T.S. and all other authors. All authors discussed the results.

## Competing interests

The authors declare no competing interests.

## Additional information

**Supplementary information** is available for this paper at https://doi.org/10.1038/s41567-018-0097-9.

**Reprints and permissions information** is available at www.nature.com/reprints.

**Correspondence and requests for materials** should be addressed to S.E.d.G.

**Publisher's note:** Springer Nature remains neutral with regard to jurisdictional claims in published maps and institutional affiliations.

## Methods

**Thin-film technology.** The NbN thin films were deposited on undoped Si(100) by plasma-enhanced atomic layer deposition (PEALD). An OpAL ALD system from Oxford Instruments Plasma Technology upgraded with a remote plasma source (ICP) and a nitrogen glove box were used. The metal–organic compound (tertbutylimido)-tris (diethylamino)-niobium (TBTDEN) and an hydrogen plasma were applied as precursors. The NbN ALD process is based on a self-limiting surface reaction principle with a well-controlled layer growth of 0.46 Å per cycle. Thus, for the CQUID experiments, superconducting NbN layers of only 3.3 nm thickness were prepared within an ALD process of 72 cycles. The prepared layers have a granular film structure. More details are given in refs [33,35] and the Supplementary Material. The precise adjustment of chemical composition, crystal structure and film thickness allows production of NbN layers with the above-reported high values of $T_c$, $R_\square$ and $L_\square$, which are essential for realizing the CQUID.

**Device fabrication.** To pattern the CQUID device we used electron beam (e-beam) lithography. A 50 nm layer of the negative e-beam resist hydrogen silsesquioxane (HSQ) was exposed to a 50 keV beam in a JEOL JBX-5500ZD e-beam lithography system. The resonator, the loops and the islands, as well as the gate electrodes, are exposed to a dose of 900 μC cm$^{-2}$ while the constrictions are defined by doses between 8.6 mC cm$^{-2}$ and 31.5 mC cm$^{-2}$. This gives constriction widths in the range 50–70 nm. After the HSQ development (MicroChemicals AZ 726 MIF), the coplanar ground-planes and the microwave and bias gate pads are defined by optical lithography using a standard lift-off technique. The ground planes and contact pads are made by thermal evaporation of a 5 nm titanium (Ti) adhesion layer and an 80 nm gold (Au) layer in a Plassys MEB 550 S evaporator. During this step, the resonator and the loops with constrictions are protected by the optical resist. After lift-off, the resonator and the loops with constrictions, islands and gates are defined in the NbN film by reactive ion etching (RIE) using an Oxford Instruments Plasmalab 80 Plus. The HSQ acts as a hard mask against the reactant fluorine ($CF_4$:Ar, 10:1) in the RIE process, which etches the NbN much faster than the HSQ. All Au-covered areas are protected since Au is inert against fluorine RIE. Test structures for d.c. measurements were co-fabricated on the same films, from which we extract values for $T_c$ and $R_\square$ measured just above $T_c$.

**Measurements.** Samples were mounted in a dilution refrigerator with a base temperature of 20 mK, essential for maximizing the coherence of the device and minimizing the effect of thermally activated phase slips. Samples were shielded by both superconducting and Cryoperm shields to minimize noise in the flux threading the loops. Heavily attenuated coaxial lines were used for microwave excitation and the transmitted signal was passed through two cryogenic isolators before being amplified by a cryogenic high-electron-mobility transistor amplifier at 4 K. The gate voltages were applied through low-pass filtering Thermocoax lines, with additional low-pass filtering at the mixing chamber stage. The measured gate period ($2e$) at the sample was 60.1 mV, giving an effective gate capacitance of 5 aF, in good agreement with finite-element electrostatic calculations of the total capacitance as seen by the island of 20 aF, which also includes the contributions from the gate capacitance. The dispersive readout of the resonator is performed by applying a weak probe tone at the fundamental resonance frequency of 3.74 GHz that monitors the phase shift of the resonator (using a vector network analyser) in response to a strong tone that induces transitions in the loop's energy spectrum. The particular loop presented in this manuscript was identified by its flux periodicity, matched to the designed loop area. This particular sample had six loops with working constrictions, allowing for easy identification.

**Data availability.** Experimental data is available from the corresponding author upon reasonable request.